# Effective Measures to Improve Current Collection Quality for Double Pantographs and Catenary Based on Wave Propagation Analysis

Zhao Xu, *Student Member, IEEE*, Yang Song, *Member, IEEE*, and Zhigang Liu, *Senior Member, IEEE*

*Abstract*—The pantograph installed on the train roof is responsible for collecting the electrical energy via the sliding contact with the catenary constructed along the railroad. To enhance the carrying capacity of the high-speed train, multiple pantographs are normally mounted on the EMU (Electrical Multiple Unit train) to interact simultaneously with the catenary. Especially in China, the double pantographs-catenary interaction is gradually becoming the mainstream in the newly built high-speed network. The biggest challenge of double-pantograph operation is the deterioration of the current collection quality of the trailing pantograph. The mechanical wave excited by the leading pantograph propagates along the contact wire and disturbs the trailing pantograph. This paper attempts to propose effective measures to improve the current collection quality of the trailing pantograph. To improve the understanding of the wave propagation in the contact wire excited by two pantographs, the double pantographs-catenary model is established using a FEM (Finite Element Method) approach. Through the analysis of the contact wire uplift response excited by a single moving force, the optimal interval of double pantographs is discussed. The results indicate that the bad interval appears at the velocity peak of the contact wire uplift, whereas, the good interval appears at the valley value of the contact wire uplift velocity. Based on this idea, the formula of optimal interval of double pantographs is proposed, and its validity is verified using the parameters of the European and China high-speed networks. Then the damper is introduced to the steady arm to reduce the wave intensity. The simulation results show that the slight steady arm damping has a positive effect on the performance of the double pantographs-catenary interaction.

*Index Terms*— Pantograph-catenary interaction, double-pantographs operation, FEM, wave propagation, optimization.

## I. INTRODUCTION

IN China, the demand for the huge pressure of population migration (Especially during the Spring Festival) greatly challenges the carrying capacity of the high-speed railway. In order to increase the carrying capacity of the high-speed train, the two EMUs are normally connected in some newly-built high-speed lines. In this circumstance, the high-speed trains are equipped with double pantographs to collect the electric current from the catenary, as shown in Fig. 1. Which brings some new technical challenges. One of them is the deterioration of the current collection quality of the trailing pantograph, which is normally caused by the wave propagation in the contact wire. The mechanical wave excited by the leading pantograph propagates backwards, and disturbs the contact quality of the trailing pantograph. Apart from China, the double-pantograph operation has been widely adopted in the high-speed networks around the world, such as Japan and Europe, to ensure sufficient energy transmission from the catenary to the locomotive. The improvement of the trailing pantograph current collection quality has been an urgent issue around the world.

As the only source of power to the locomotive, the interaction performance of pantograph-catenary system has attracted wide attention of many scholars. In order to study the dynamic performance, simulation tools are very common measures [1], [2], even on higher speed AHV (Air-breathing hypersonic vehicle) [3], [4]. The most ten distinguished ones are compared to set up the benchmark for the validation of numerical simulation of pantograph-catenary interaction [5]. Among them, the catenary is usually modelled by the nonlinear finite element approach [6], and the pantograph is normally represented by a multibody or lump-mass model [7]. The measurement data is also collected to validate the validity of numerical models [8]. In order to improve the computational efficiency, the moving mesh method [9], [10] and modal coordinate model [11] are widely used. The importance of damping to improve to structural performance has been widely acknowledged [12]. The damping properties are identified by covariance-driven stochastic subspace identification (Cov-SSI) method [13] and the noncontact measurement technique [14]. Normally the pantograph-catenary interaction is affected by the disturbance from both of the external environment and the system itself. Some researchers investigate the effect of external disturbance, such as the wind load [15], [16], the aerodynamic instability [17], the locomotive excitation [18], the electromagnetic interference [19], and the temperature variation [20] on the pantograph-catenary interaction. The internal disturbance normally includes the wave propagation in the contact wire [21], the anomaly of components [22], and the wear and irregularities

Z. Xu and Z. Liu are with the School of Electrical Engineering, Southwest Jiaotong University, Chengdu 610031, China (E-mail: xuzhao94@foxmail.com liuzg_cd@126.com).

Y. Song is with the Department of Structural Engineering, Norwegian University of Science and Technology, 7491 Trondheim, Norway (E-mail: y.song_ac@hotmail.com).
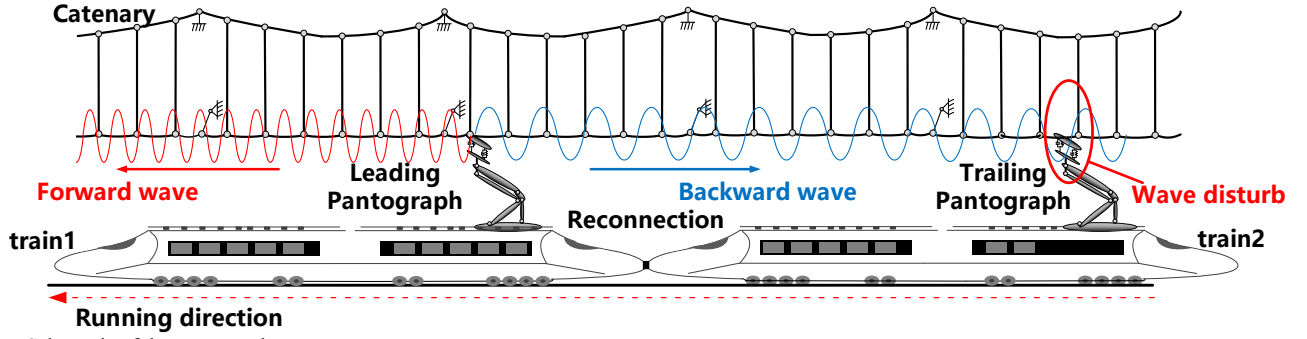
Fig. 1.  Schematic of the pantograph-catenary system.

in the contact wire [23]. Some control strategies [24]–[26] are proposed to limit these negative effect on the current collection quality.

Recently, the performance of the catenary interacting with multiple pantographs has been concerned by some researchers. The important implication of mechanical waves excited by the leading pantograph to the contact performance of trailing pantograph has been indicated in [27], [28]. The disturbance of the wave excited by leading pantograph to the trailing pantograph is investigated in detail [29], [30]. Basically there are two measures to improve the trailing pantograph performance. One is to place the trailing pantograph in the right position, which cannot be disturbed largely by the wave of the leading pantograph. The other is to reduce the intensity of the mechanical wave of the leading pantograph, and eliminate its effect on the trailing pantograph. Based on the former idea, two formulas of optimal interval for double pantographs are proposed in [29] and [30]. However, according to the analysis in Section III, these two measures are not perfectly consistent with the simulation results. The effectiveness of the second measure has not been investigated in any published literature. Thus, the main aim of this paper is to modify the formula of optimal interval addressing the shortcomings of the previous work, and investigate the effect of damping components on the improvement of the trailing pantograph performance.

In this paper, a double pantograph-catenary interaction model is presented, and the validation is verified by comparison with the benchmark (in Section II). Then a China high-speed network is taken as the analysis object, and the applicability of previous solutions for the optimal interval of double pantographs is investigated. The shortfalls of previous solutions are drawn (in Section III). The wave propagation from the leading pantograph to the trailing pantograph is analysed by numerical simulations, and the new formula for the optimal interval is proposed (in Section IV). Through a number of simulations, the validation of the proposed formula is verified on both of the China and European high-speed networks. At last, the damping components are included in the catenary to eliminate the negative effect of wave propagation on the trailing pantograph. The effect of the steady arm damping on the trailing pantograph contact force is quantified.

## II. MODELLING OF DOUBLE PANTOGRAPHS-CATENARY SYSTEM

This section presents the catenary model used in the subsequent analysis. The catenary is modelled by FEM, and the pantographs are represented by the lumped-mass model. The latest European standard EN 50318:2018 [31] is adopted to verify the validation of the present model.

### A. Modelling of catenary

The catenary is normally comprised of the contact wire, the messenger wire, the steady arm, the messenger wire support and several droppers and clamps in each span, as shown in Fig. 2.

In order to fully describe the geometrical nonlinearity, the Euler-Bernoulli beam is adopted to model the contact wire, the messenger and the steady arm. The nonlinear truss element is adopted to model the dropper. All the clamps are taken as lumped masses. According to the finite element method, the equation of motion for the catenary is written as

$$\mathbf{M}_C \ddot{\mathbf{U}}_C + \mathbf{C}_C \dot{\mathbf{U}}_C + \mathbf{K}_C \mathbf{U}_C = \mathbf{F}_C \qquad (1)$$

in which, $\ddot{\mathbf{U}}_C$, $\dot{\mathbf{U}}_C$ and $\mathbf{U}_C$ are the global acceleration, velocity and displacement vectors of the catenary respectively. $\mathbf{F}_C$ is the external force vector applied on the catenary. The mass matrix $\mathbf{M}_C$ and the stiffness matrix $\mathbf{K}_C$ are assembled by the element matrix of each catenary component as follows [32]:

$$\mathbf{M}_C = \sum_{n_{cw}} \mathbf{M}_{cw,n}^e + \sum_{n_{mw}} \mathbf{M}_{mw,n}^e + \sum_{n_{dr}} \mathbf{M}_{dr,n}^e + \sum_{n_{cs}} \mathbf{M}_{cs,n}^e + \sum_{n_{cl}} \mathbf{M}_{cl,n}^e$$

$$\mathbf{K}_C = \sum_{n_{cw}} \mathbf{K}_{cw,n}^e + \sum_{n_{mw}} \mathbf{K}_{mw,n}^e + \sum_{n_{dr}} \mathbf{K}_{dr,n}^e + \sum_{n_{cs}} \mathbf{K}_{cs,n}^e + \sum_{n_{ms}} \mathbf{K}_{ms,n}^e \qquad (2)$$

in which, $\mathbf{M}_{cw,n}^e$ is the element mass matrix of contact wire, which is expressed by

$$\mathbf{M}_{cw,n}^e = \sum \rho_{cw} A_{cw} \int_0^{l_e} \mathbf{N}_x^{r\,T} \mathbf{N}_x^r dx + \rho_{cw} A_{cw} \int_0^{l_e} \mathbf{N}_y^{r\,T} \mathbf{N}_y^r dx$$
$$+ \rho_{cw} A_{cw} \int_0^{l_e} \mathbf{N}_z^{r\,T} \mathbf{N}_z^r dx + \rho_{cw} W_r \int_0^{l_e} \mathbf{N}_{\theta x}^{r\,T} \mathbf{N}_{\theta x}^r dx \qquad (3)$$

in which, $\rho_{cw}$ and $A_{cw}$ are the linear density and the sectional area of the contact wire. $W_r$ is the polar moment of inertial of the contact wire cross-section. $l_e$ is the element
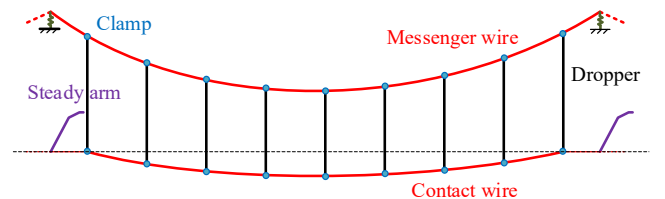


Fig. 2.  Schematic of catenary.

length of the contact wire. $\mathbf{N}_x^r$, $\mathbf{N}_y^r$, $\mathbf{N}_z^r$ and $\mathbf{N}_{\theta x}^r$ are the shape functions of the Bernoulli beam along the $X$-, $Y$- and $Z$-axis and around the $X$-axis, respectively. $\mathbf{M}_{mw,n}^e$ is the element mass matrix of messenger wire, which is similar to $\mathbf{M}_{cw,n}^e$. Only the subscript is changed to 'mw'. $\mathbf{M}_{dr,n}^e$ is the element mass matrix of dropper, which is expressed by

$$\mathbf{M}_{dr,n}^e = \sum \rho_{dr} A_{dr} \int_0^{l_e} \mathbf{N}_x^{dT} \mathbf{N}_x^d dx + \rho_{dr} A_{dr} \int_0^{l_e} \mathbf{N}_y^{dT} \mathbf{N}_y^d dx + \rho_{dr} A_{dr} \int_0^{l_e} \mathbf{N}_z^{dT} \mathbf{N}_z^d dx \quad (4)$$

in which, $\rho_{dr}$ and $A_{dr}$ are the linear density and the sectional area of the dropper. $\mathbf{N}_x^d$, $\mathbf{N}_y^d$ and $\mathbf{N}_z^d$ are the shape functions of the truss element along the $X$-, $Y$- and $Z$- axis, respectively. The truss element is also used to describe the steady arm. So the steady arm element mass matrix $\mathbf{M}_{cs,n}^e$ is similar to $\mathbf{M}_{dr,n}^e$. Only the subscript changes to 'cs'. $\mathbf{M}_{cl,n}^e$ denotes the element mass matrix of claw, which is a diagonal matrix.

Similarly, the element stiffness matrix $\mathbf{K}_{cw,n}^e$ is the element stiffness matrix of contact wire, which is written by

$$\begin{cases} \mathbf{K}_{cw,n}^e = \mathbf{K}_\alpha + \mathbf{K}_\beta + \mathbf{K}_\chi + \mathbf{K}_\delta \\ \mathbf{K}_\alpha = \sum E_{cw} A_{cw} \int_0^{l_e} \left( \dfrac{\partial \mathbf{N}_x^r}{\partial x} \right)^T \dfrac{\partial \mathbf{N}_x^r}{\partial x} dx \\ \mathbf{K}_\beta = E_{cw} I_{cwy} \int_0^{l_e} \left( \dfrac{\partial^2 \mathbf{N}_x^r}{\partial x^2} \right)^T \dfrac{\partial^2 \mathbf{N}_x^r}{\partial x^2} dx \\ \mathbf{K}_\chi = E_{rw} I_{cwz} \int_0^{l_e} \left( \dfrac{\partial^2 \mathbf{N}_y^r}{\partial x^2} \right)^T \dfrac{\partial^2 \mathbf{N}_y^r}{\partial x^2} dx \\ \mathbf{K}_\delta = G_{cw} I_{cwx} \int_0^{l_e} \left( \dfrac{\partial^2 \mathbf{N}_{\theta x}^r}{\partial x^2} \right)^T \dfrac{\partial^2 \mathbf{N}_{\theta x}^r}{\partial x^2} dx \end{cases} \quad (5)$$

in which, $E_{cw}$ is the Young's modulus of the contact wire. $I_{cwx}$, $I_{cwy}$ and $I_{cwz}$ are the inertial moment of the contact wire with respect to the $X$-, $Y$- and $Z$- axis. $G_{cw}$ is the rigid modulus of the contact wire. $\mathbf{K}_{mw,n}^e$ is the element stiffness matrix of messenger wire, which is similar to $\mathbf{K}_{cw,n}^e$. Only the subscript changes to 'mw'. $\mathbf{K}_{dr,n}^e$ is the element stiffness matrix of dropper, which is expressed by

$$\mathbf{K}_{dr,n}^e = \sum E_{dr} A_{dr} \int_0^{l_e} \left( \dfrac{\partial \mathbf{N}_x^d}{\partial x} \right)^T \dfrac{\partial \mathbf{N}_x^d}{\partial x} dx \quad (6)$$

in which, $E_{dr}$ is the Young's modulus of dropper. The dropper can only withstand the tension but not the compression. The dropper stiffness changes to 0 N/m when it works in compression. As the same element is used to describe the steady arm, so steady arm element stiffness matrix $\mathbf{K}_{cs,n}^e$ has the same form with $\mathbf{K}_{dr,n}^e$. Only the subscript changes to 'cs'. $\mathbf{K}_{ms,n}^e$ denotes the element stiffness matrix of messenger wire support, which is taken as virtual support point with equivalent lumped stiffness.

The structural damping matrix $\mathbf{C}_C$ is introduced according to the proportional damping assumption, that is, in the following form [13]:

$$\mathbf{C}_C = \alpha \mathbf{M}_C + \beta \mathbf{K}_C \quad (7)$$

where $\alpha$ and $\beta$ are two constant values derived from the experimental measurement.

### B. Modelling of pantograph

In this work, the pantograph is represented by a widely used lumped-mass model. Normally the equivalent physical parameters including the mass, stiffness and damping are derived though the bench test. It is well acknowledged that the lumped mass model has a good performance to describe the physical characteristics of a realistic pantograph. The contact between the pantograph collector and contact wire is described by the penalty function method as shown in Eq. (8).

$$f_c = \begin{cases} k_c \left( y_p - y_c \right) & y_p \geq y_c \\ 0 & y_p < y_c \end{cases} \quad (8)$$

in which, $f_c$ is the contact force between the contact wire and pantograph collector. $y_p$ is the vertical displacement of pantograph collector and $y_c$ is the vertical displacement of contact point in the contact wire. $k_c$ is the contact stiffness.

### C. Model verification

In order to gain the confidence of the subsequent analysis, the newest EN 50318 released in 2018 is adopted to verify the validation of the present model. In the newest standard, a reference model of double pantographs-catenary is firstly introduced to verify the validation of simulation tools. The parameters of the reference model in the standard are shown in Fig. 2 and Table 1. In this simulation, the vehicle speeds are set to 275 km/h and 320 km/h, and the interval between two pantographs is set to 200 m, according to the requirement in EN 50318. Table 2 presents the results of the catenary static configuration and the percentage error with respect to the standard value. It is seen that the contact wire pre-sag in the mid-span is 54.9 mm, which has a small percentage error of 0.18% with respect to the standard value. The maximum error of pre-sag in the dropper and support points only reaches 0.96%, which is significantly lower than the threshold of 10%. As for the equivalent elasticity, which is obtained by applying a constant moving vertical force of 200 N on the contact wire, the maximum percentage error is only 3.22%. Table 3 shows the comparison of the dynamic results with respect to the standard acceptance range. It is seen that the results perfectly fall within the range of acceptance, which means that the present model has the convincible accuracy to perform the further analysis.

### III. PREVIOUS SOLUTION AND SHORTFALLS

According to the literature review to the previous researches, the traditional solution is to place the trailing pantograph at the right position, where the disturbance of the mechanical wave of leading pantograph is not intense. Based on this idea, two formulas are proposed for the optimal interval of the double pantographs. In this section, the validations of these formulas

TABLE I.
GEOMETRICAL PROPERTIES OF CATENARY

| Catenary material property | |
|---|---|
| Contact wire(CW) | Line density: 1.35 kg/m; Tension: 22 kN; Young's modulus: 100 kN/mm$^2$; Cross section; 150 mm$^2$ |
| Messenger wire(MW) | Line density: 1.08 kg/m; Tension: 16 kN; Young's modulus: 97 kN/mm$^2$; Cross section; 120 mm$^2$ |
| Dropper | Line density: 0.117 kg/m; Clamp mass; 195 g (on CW), 165 g (on MW) Tensile rigidity from dropper1 to 9 (kN/m): 197; 223; 247; 264; 269; 264; 247; 223; 197; |
| Steady arm | Line density: 0.739 kg/m |
| MW support | Stiffness: 500 kN/m; Damping: 1000 Ns/m |
| Catenary geometrical property | |
| Encumbrance:1.2 m; Interval of droppers: 6.25 m; Number of droppers: 9; Number of span: 29; Length of span 50 m; Stagger value: 0.2 m; Steady arm length: 1.2 m; | |

TABLE II.
RESULTS OF STATICALLY SHAPE FINDING

| | Pre-sag [mm] | Result [mm] | Percentage error [%] | $e$ [mm/N] | Result [mm/N] | Percentage error [%] |
|---|---|---|---|---|---|---|
| Support | 0 | 2.7e-7 | 0 | 0.206 | 0.2002 | 2.82 |
| 1 | 0 | 0 | 0 | 0.165 | 0.1649 | 0.06 |
| 2 | 24 | 24.1 | 0.41 | 0.273 | 0.2818 | 3.22 |
| 3 | 41 | 41.2 | 0.49 | 0.345 | 0.3519 | 2.00 |
| 4 | 52 | 51.5 | 0.96 | 0.388 | 0.3934 | 1.39 |
| 5 | 55 | 54.9 | 0.18 | 0.400 | 0.4072 | 1.8 |
| 6 | 52 | 51.5 | 0.96 | 0.388 | 0.3934 | 1.39 |
| 7 | 41 | 41.2 | 0.49 | 0.345 | 0.3519 | 2.00 |
| 8 | 24 | 24.1 | 0.41 | 0.273 | 0.2818 | 3.22 |
| 9 | 0 | 0 | 0 | 0.165 | 0.1649 | 0.06 |
| Support | 0 | 2.7e-7 | 0 | 0.206 | 0.2002 | 2.82 |

TABLE III.
RESULTS OF DYNAMIC SIMULATIONS.

| Speed | 275 | | | |
|---|---|---|---|---|
| Pantograph | 1 | | 2 | |
| | Range of acceptance | Result | Range of acceptance | Result |
| $F_m$ [N] | 141.5-146.5 | 143.1 | 141.5-146.5 | 144.4 |
| $\sigma$ [N] | 31.9-34.8 | 33.3 | 50.0-54.5 | 51.6 |
| $\sigma$ (0-5Hz) [N][b] | 26.4-28.9 | 27.2 | 41.2-45.4 | 42.8 |
| $\sigma$ (5-20Hz) [N][b] | 16.2-22.4 | 19.3 | 25.2-34.7 | 29.3 |
| $F_{max}$ [N] | 211.9-244 | 222.9 | 241-290 | 260.4 |
| $F_{min}$ [N] | 71-86 | 85.8 | 14-50 | 34.5 |
| Speed | 320 | | | |
| Pantograph | 1 | | 2 | |
| | Range of acceptance | Result | Range of acceptance | Result |
| $F_m$ [N] | 166.5-171.5 | 169.4 | 166.5-171.5 | 168.8 |
| $\sigma$ [N] | 49.5-62.9 | 53.7 | 30.2-43.8 | 42.3 |
| $\sigma$ (0-5Hz) [N][b] | 38.7-44.4 | 40.1 | 14.3-23.3 | 19.0 |
| $\sigma$ (5-20Hz) [N][b] | 29.0-46.2 | 35.7 | 29.0-46.2 | 37.9 |
| $F_{max}$ [N] | 295-343 | 295.0 | 252-317 | 269.5 |
| $F_{min}$ [N] | 55-82 | 60.0 | 51-86 | 59.7 |

are evaluated, and the shortfalls in previous researches and potential solutions are discussed.

*A. Problem description*

In 2008, the opening of the intercity line between Beijing and Tianjin marked the rapid expansion of China high-speed network in the last decade. However, the EMUs running on the Beijing-Tianjin high-speed line are only equipped with a single pantograph in the last decade. In order to increase the carrying capability, CRC (China Railway Corporation) asks to explores the potential to run double pantographs in the existing line. In

this section, the catenary of Beijing-Tianjin railway with double pantographs is taken as the analysis object to check the validation of previous formulas for optimal pantograph interval, and investigate the potential solution for improving the current collection quality of trailing pantograph. Using the method described in Section II, the double pantographs-catenary model is established, the parameters of which are presented in Table 4 and Fig. 3. The pantograph running speed is set to the maximum design speed of the catenary 350 km/h, and the distance between the two pantographs is gradually increased from 95 m
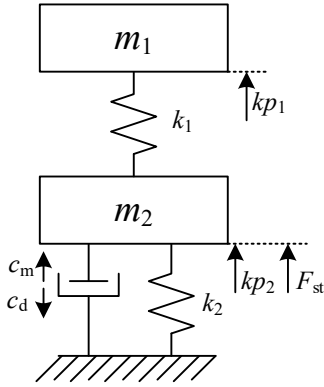
Fig. 3.    Pantograph model.

TABLE IV.
PARAMETERS OF PANTOGRAPH-CATENARY MODEL
(BEIJING-TIANJIN HIGH-SPEED LINE)

| Catenary material property | |
|---|---|
| Contact wire(CW) | Line density: 1.082 kg/m; Tension: 27 kN; Young's modulus: **100** kN/mm²; Cross section; 120 mm² |
| Messenger wire(MW) | Line density: 1.068 kg/m; Tension: 21 kN; Young's modulus: **97** kN/mm²; Cross section; 120 mm² |
| Dropper | Tensile rigidity: 105 N/m |
| MW support | Fixed |
| **Catenary geometrical property** | |
| Encumbrance:1.6 m; Interval of droppers: 10 m; Number of droppers: 5; Number of span: 29;Length of span 50 m; Stagger value: 0.3 m; Steady arm stiffness: $1.25 \times 10^7$ N/m; | |
| **Pantograph property** | |
| $m_1$: 5 kg; $m_2$: 18.98 kg; $k_1$: 6000 N/m; $k_2$: 0.5 N/m; $c_m$: 5 Ns/m; $c_d$: 350 Ns/m; $kp_1$: 0.006 Ns²/m²; $kp_2$: 0.006 Ns²/m²;$F_{st}$: 70 N. | |

to 320 m. The contact force standard deviation of the trailing pantograph is selected as the indicators to evaluate the current collection quality, as it directly reflects the fluctuation and dispersion of contact force around its mean value [33]. The resulting contact force standard deviations versus pantograph interval are shown in Fig. 4. It is seen that the standard deviation changes periodically versus the pantograph interval.

*B.  Previous solution*

In order to explain this periodic relationship between the contact force standard deviation and the pantograph interval, Zhang et al. [29] and Liu et al. [30] analyze the wave propagation in the contact wire interacting with double pantographs. In Zhang et al's work, the good performance can be obtained, when the mechanical wave phase of leading pantograph is opposite to that of the trailing pantograph. The formula for optimal interval is given as follows

$$L_p = \begin{cases} (2k+1)\dfrac{Lu}{\alpha\sqrt{T/\rho}}, k=1,2,3\cdots & \text{(Optimal interval)} \\ 2k\dfrac{Lu}{\alpha\sqrt{T/\rho}}, k=1,2,3\cdots & \text{(Bad interval)} \end{cases} \quad (9)$$

in which, $L$ is the span length of the catenary, $u$ is the velocity of the train, $\alpha$ is the correction factor, $T$ is the tension of the contact wire and $\rho$ is the line density of contact wire. According to Zhang et al.'s method, at 350 km/h, the optimal intervals between the leading and trailing pantographs $L_p$ for the Beijing-Tianjin high-speed line are 92.3 m, 153.9 m, 215.4 m, 277.0 m
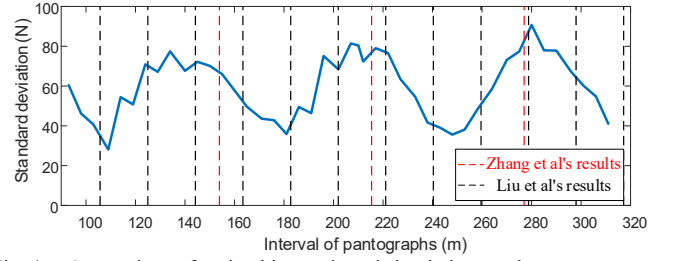


Fig. 4.    Comparison of optimal intervals and simulation results

($k = 1, 2, 3\ 4$), and the bad intervals are 61.5 m, 123.1 m, 184.6 m, 246.2 m. The other optimal formula is suggested by Liu et al. [30] based on the wave interference theory, which is expressed by

$$L_p = \left(\frac{3}{2}+k\right)\frac{(C-u)L}{C}, k=1,2,3\cdots \quad (10)$$

in which, $C$ is the wave propagation speed. The optimal pantograph intervals calculated by the two previous formulas are plotted in dash lines in Fig. 4. The red dash lines represent the resulting optimal intervals calculated by Eq. (9), and the black dash lines denote the results calculated by Eq. (10). Significant shortcomings can be observed in Fig. 4. Most red lines do not appear at the positions of optimal interval. Even though some black dash lines appear at the same positions of the local least standard deviations, Eq. (10) gives many non-optimal intervals of double pantographs. In Liu et al.'s work, they use the leading pantograph as an auxiliary pantograph, which does not collect any electric current, to minimise the negative effects caused by the leading pantograph at very short pantograph intervals. The physical meaning of this shorter interval is the distance between a certain point in the contact wire and the pantograph when the point reaches the first valley after the pantograph passes. Liu et al.'s formula results in a lot of good intervals with very small spacing, but only the first solution is valid. However, in Zhang et al.'s formula, the wave frequency of leading pantograph is simply calculated by the wave speed and the span length, and a modified coefficient $\alpha$ is introduced for different structural types of catenary. In addition, Zhang et al.'s work assumes the stable vibration of the contact wire during the entire process of pantograph passing. However, the contact wire is not always in a stable vibration. During the short period when the pantograph passes, the contact wire experiences a significant forced-vibration. So, previous optimal interval formulas are not perfectly consistent with the simulation results, which cannot provide good solutions for improving the current collection quality of trailing pantograph. In order to overcome the shortfalls of the previous solution, a new method needs to be proposed to improve current collection quality for trailing pantographs

*C.  Potential solution*

Through the analysis of Fig. 4, it is found that compared with Eq. (10), the results of Eq. (9) show a similar periodicity with the simulation results. However, the optimal intervals obtained by Eq. (9) are not consistent with the simulation results. Actually Eq. (9) is closer to the non-optimal interval of the simulation results. Eq. (10) mainly focuses on the small interval

of double pantographs, which cannot provide useful information for large pantograph interval used in China high-speed network. Therefore, the idea of Zhang et al.'s work is adopted in this work to propose a new valid formula for the optimal double pantographs interval. It is assumed that the response of the contact wire uplift response caused by single pantograph may contain some useful information, which can be used to reveal the deterioration mechanism of the current collection quality of the trailing pantograph. This work conducts a thorough investigation on the response of the contact wire uplift with the excitation of a single pantograph. Based on the analysis results, the trailing pantograph is placed at the right position for a better current collection quality. Then the formula of the optimal interval of double pantographs is updated, and its validation is verified through a number of numerical examples.

## IV. MECHANISM OF DETERIORATION OF TRAILING PANTOGRAPH CURRENT COLLECTION QUALITY

In order to study the deterioration mechanism of the trailing pantograph current collection quality, a number of simulations of the double pantographs-catenary interaction are done with different speeds and pantograph intervals, using the parameters of the Beijing-Tianjin high-speed line. The speed varies from 300 km/h to 380 km/h, and the interval is from 130 m to 250 m. The resulting contact force standard deviations of trailing

pantograph versus pantograph interval and speed are shown in Fig. 5. It is seen that the periodic relationship between the standard deviation and the interval is affected by the speed. Specifically, as the speed increases, the period of the standard deviation versus the pantograph interval increases.

In order to further investigate the deterioration mechanism of the trailing pantograph current collection quality, a moving force of 150 N is applied on the catenary. The contour of resulting contact wire uplift versus the position and time at 350 km/h is shown in Fig. 6, in which the red line denotes the trajectory of the moving force; the yellow line describes the propagation of forward wave; and the white line represents the propagation of backward wave. The red ellipse indicates the post-passage uplift response of a point in the contact wire after the constant force passes. Due to the Doppler effect, the amplitude of the forward propagating wave is much smaller than that of the backward propagating wave. That is why the backward propagating wave of leading pantograph has significant effect on the trailing pantograph. According to Fig. 4, a optimal interval (177 m) and a bad interval (135 m) are
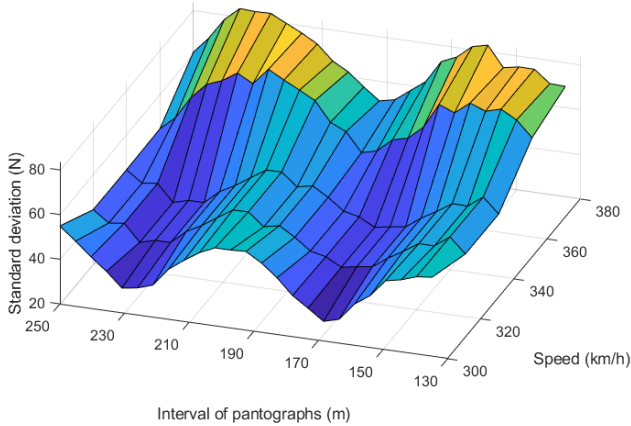


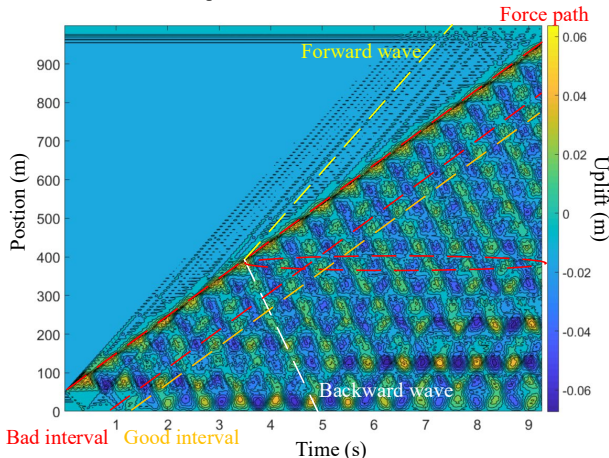Fig. 5. Standard deviations of the contact force of trailing pantograph results in different intervals and speeds



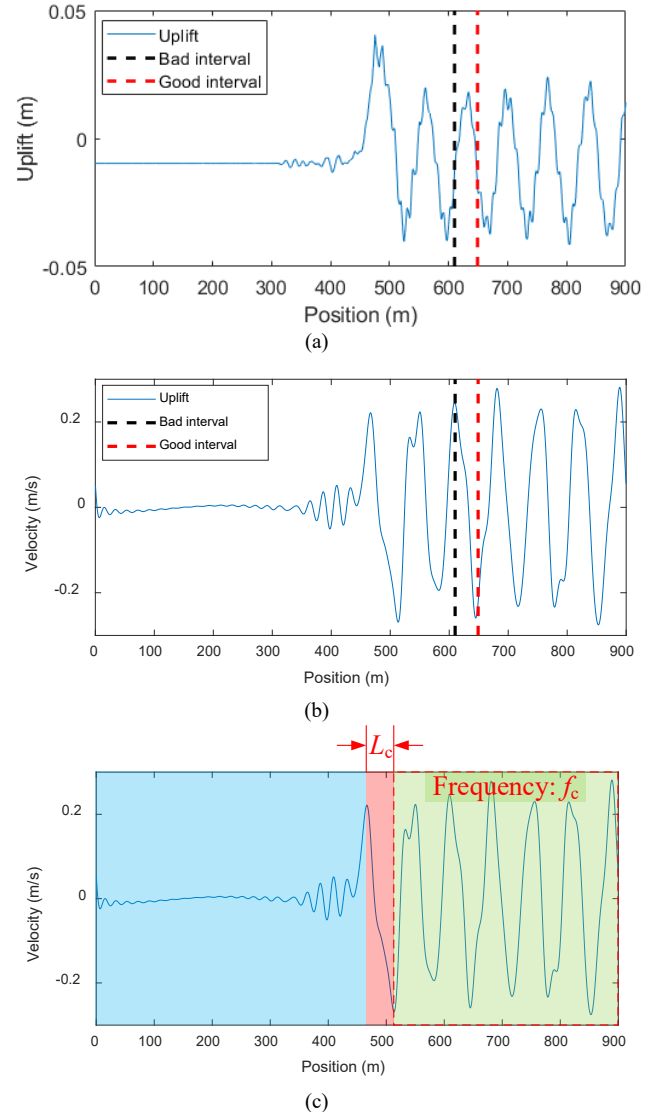Fig. 6. Vibration of the contact wire at the speed of 350km/h.



Fig. 7. (a) Uplift of contact wire; (b) Velocity of contact wire; (c) Partition of the velocity.

taken as the analysis object, which are denoted by the red and yellow dash lines in Fig. 6. The uplift response at the contact wire support point is extracted from Fig. 6, as shown in Fig. 7(a). The velocity of the response is presented in Fig. 7(b) by differentiating Fig. 7(a). It is seen that bad interval coincidently appears at the velocity peak of the contact wire uplift. On the contrary, the optimal interval appears at the valley value of the contact wire uplift velocity. It can be explained that when the trailing pantograph is placed at the velocity peak of the contact wire uplift caused by the leading pantograph, the resonance may occur and cause the deterioration of the current collection quality. When the trailing pantograph is placed at the valley value of the contact wire uplift velocity, the vibration will be offset and attenuate the effects of the leading pantograph. Therefore, the current collection quality of the trailing pantograph is improved.

To summarize the formula for the optimal interval, the positions of the velocity valley and peak of the contact wire uplift should be investigated. Fig. 7 (c) divides the response into three stages. The first is the pre-passage stage shown in the blue background. In this region, the contact wire is subjected to the forward wave causing slight oscillations. At the time when the moving force is approaching, the velocity reaches the maximum. The second one is the passing stage shown in the red background. At this time when the moving force passes the support point, the velocity increases to the maximum and sharply reduced to the minimum. The length of the red region is denoted by $L_c$. The last one is the post-passage stage, as shown in the green background. The contact wire is affected by the backward wave, and the velocity exhibits periodic fluctuation. The fluctuation frequency in this stage is denoted by $f_c$. According to the above analysis, when resonance occurs, the trailing pantograph appears at the peak of the contact wire uplift velocity. Under this circumstance, the relationship between the interval of double pantographs and the running speed can be expressed by Eq. (11).

$$\frac{v}{L_p - L_c} = \frac{2}{2k-1} f_c \qquad (11)$$

in which, the $v$ is the train speed. $L_p$ is the interval of pantographs. When Eq. (11) is satisfied, $L_p$ is the bad interval. On the contrary, when the trailing pantograph appears at the valley of the velocity, the formula for optimal intervals can be derived. The formulas for both the optimal and bad intervals are summarised as follows:

$$L_p = \begin{cases} \dfrac{2k-1}{2} \cdot \dfrac{v}{f_c} + L_c & k=1,2,3....... \text{ Optimal intervals} \\ \\ k \cdot \dfrac{v}{f_c} + L_c & k=1,2,3....... \text{ Bad intervals} \end{cases} \qquad (12)$$

It is seen that the optimal interval is determined by the $L_c$ and $f_c$. It is necessary to investigate the potential factors affecting $L_c$ and $f_c$. The specific value of $L_c$ is related to the structure of the catenary itself and the train speed. It could be obtained by the simulation with a single pantograph. The value of $f_c$ is the fluctuation frequency of the contact wire uplift in the green background in the Fig. 7(c). The frequency analysis is
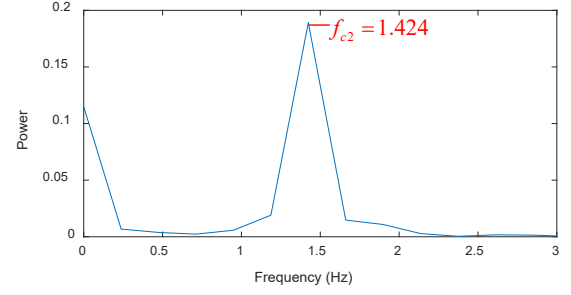


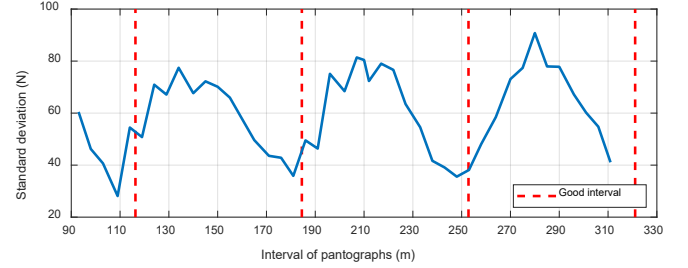Fig. 8. Frequency domain of contact wire uplift.



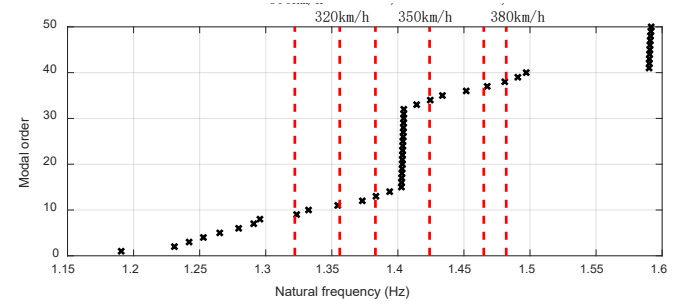Fig. 9. Comparison of optimal intervals and calculation results.



Fig. 10. Comparison of $f_c$ and natural frequency.

performed to obtain $f_c$, as shown in Fig. 8. It can be seen that at 350 km/h, the peak frequency of the contact wire appears at the mid-span position, which is 1.424 Hz. Using the Eq. (12), the optimal interval between the double pantographs at the speed of 350 km/h are 116.3 m, 184.5 m, 252.8 m, and, 321.1 m. The comparison between the calculation results and the simulation results is shown in Fig. 9. It can be seen that the optimal intervals calculated by Eq. (12) are reasonably consistent with the simulation results. Compared with Fig. 4, the proposed formula gives more accurate results than previous two methods.

In order to obtain $f_c$ and $L_c$ with higher speeds, the simulations with single moving force are performed at the speeds of 300 km/h, 320 km/h, 340 km/h, 360 km/h, and, 380 km/h, respectively. The corresponding resulting $f_c$ and $L_c$ are shown in Table 6. It can be seen that the value of the response frequency $f_c$ undergoes a slight increase with the increase of the speed. Through the mode analysis, the natural frequencies are presented in Fig. 10. Through the comparison with the natural frequency of the catenary, it is seen that $f_c$ is always consistent to one of natural frequency. It is concluded that the moving-load excitation to the catenary is able to excite one of the natural frequency of the

TABLE VI.
RESPONSE FREQUENCY AND OPTIMAL INTERVALS AT DIFFERENT
SPEEDS

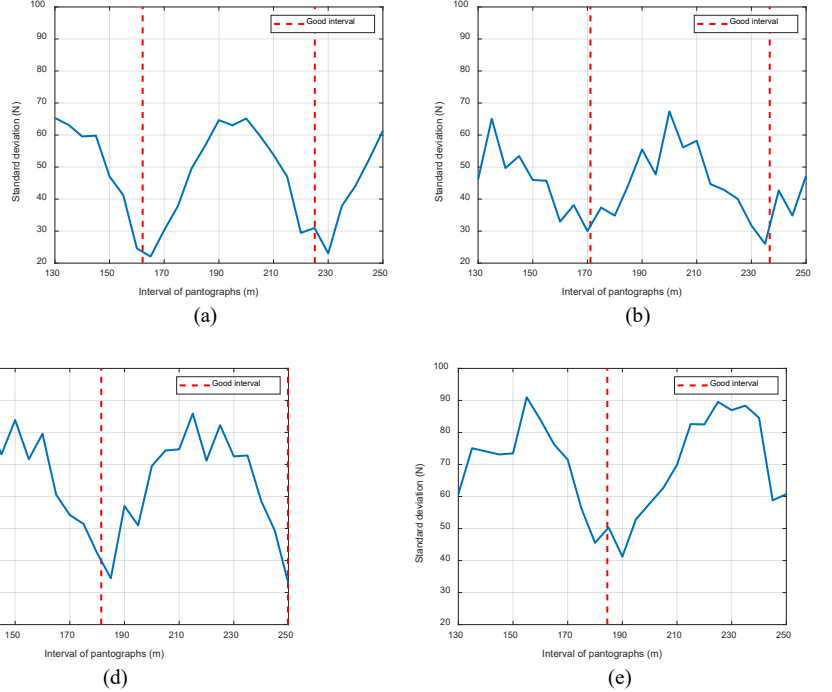| Speed (km/h) | $f_c$ (Hz) | $L_c$ (m) | Optimal intervals (m) |
|---|---|---|---|
| 300 | 1.322 | 36 | 99.0; 162.1; 225.1; 288.1 |
| 320 | 1.356 | 40 | 105.6; 171.1; 236.7; 302.1 |
| 340 | 1.383 | 37 | 105.3; 173.6; 241.9; 310.2 |
| 360 | 1.465 | 45 | 113.3; 181.5; 249.8; 318.3 |
| 380 | 1.482 | 42 | 113.2; 184.5; 255.7; 326.9 |

Fig. 11. Comparison of optimal intervals calculation results at different speed; (a)300km/h; (b)320km/h; (c)340km/h; (d)360km/h; (e)380km/h.
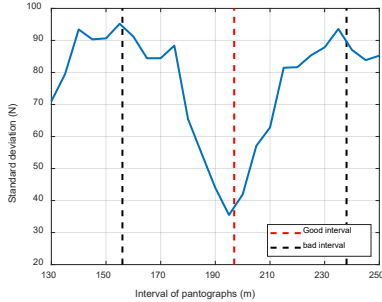
Fig. 12. Comparison of optimal interval calculation results.

TABLE VII.
RESPONSE FREQUENCY AND OPTIMAL INTERVALS AT DIFFERENT SPEEDS

| Speed (km/h) | $f_c$ (Hz) | $L_c$ (m) | Optimal intervals (m) | Bad intervals (m) |
|---|---|---|---|---|
| 320 | 1.085 | 33 | 114.9; 196.9; 278.8 | 74.0; 155.9; 237.8; 319.7 |

catenary. But the moving velocity determines which one of the natural frequencies is excited. However, the explicit relationship between the velocity and $f_c$ is still unclear, which deserves further investigations.

## V. VALIDATION

### A. Verification with Beijing-Tianjin high-speed line

In order to verify the accuracy of the formula for the optimal interval proposed in this work shown in Eq. (12), the double pantographs operation at the speeds of 300 km/h, 320 km/h, 340 km/h, 360 km/h, and, 380 km/h are simulated, the interval of pantographs increases from 130 m to 250 m. The contact force standard deviations of trailing pantograph versus $L_p$ at each speed are shown in Fig. 11. The red dash lines represent the optimal interval calculated by Eq. (12). It is seen that at different speeds, the optimal intervals of the double pantographs calculated by Eq. (12) have a good consistency with the simulation results. It is proved that the formula proposed in this work can be used to determine the optimal intervals of double pantographs.

### B. Verification with reference model in benchmark

The reference model in the benchmark, which is a realistic line from the French high-speed network, is adopted to do further validation of the proposed formula in this work. The parameters of the catenary are given in detail in Section 2.3. The norminal speed is set to 320 km/h and the distance between the two pantographs is increased from 130 m to 250 m. The resulting $f_c$ and $L_c$ are shown in Table 7, and the resulting contact force standard deviations versus $L_p$ are presented in Fig. 12. The optimal and bad intervals calculated by Eq. (12) are denoted by the red and black dash lines respectively. It is seen that both of the optimal and bad intervals obtained by the proposed formula are consistent with the simulation results. The validation of the proposed formula is verified.

The above-mentioned work proposes the formula for calculating the optimal interval of double pantographs. The post-passage contact wire uplift frequency $f_c$, and the length of passing stage $L_c$ should be determined by applying a moving excitation. Then Eq. (12) is used to calculate the optimal double pantographs interval. However, Eq. (12) is straightly relevant to the train speed and the structural parameters of the catenary. In reality, the train does not always operate at one speed, and the structure of catenary is not always identical for all spans. Therefore, the optimal interval calculated by Eq. (12) is not always the best for a real line.
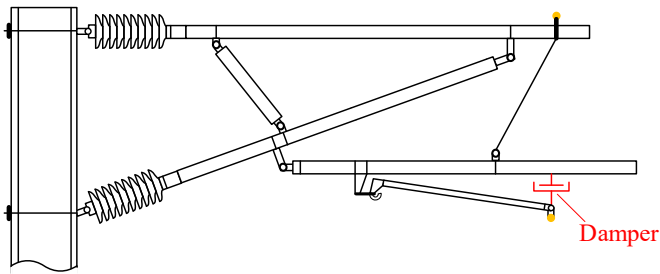
Fig. 13.    Cantilever system with damper on steady arm.

TABLE VIII.
STEADY ARM DAMPING SETTINGS AND SIMULATION RESULTS

| Damping (Ns/m) | $\sigma$(N) Leading pantograph | $\sigma$(N) Trailing pantograph | Loss contact (Y/N) |
|---|---|---|---|
| 0 | 38.27 | 71.45 | Y |
| 25 | 37.99 | 64.60 | Y |
| 50 | 39.50 | 61.15 | N |
| 75 | 41.60 | 61.29 | N |
| 100 | 43.88 | 62.58 | N |
| 125 | 46.50 | 64.76 | N |
| 150 | 49.06 | 67.39 | N |
| 175 | 51.97 | 70.75 | N |
| 200 | 54.71 | 74.06 | N |
| 225 | 57.65 | 78.10 | Y |
| 250 | 60.28 | 82.16 | Y |

## VI.    DISCUSSION OF EFFECTIVE MEASURES TO IMPROVE TRAILING PANTOGRAPH CURRENT COLLECTION QUALITY

Apart from the measure to adjust the pantographs interval, the inclusion of damping components is another normal measure to reduce the negative influence of the mechanical wave on the trailing pantograph. Previous researches only discuss the structural damping of the catenary system [13], [14]. In this section, the damper is added to the steady arm (as shown in Fig. 13) to decrease the intensity of the wave excited by the leading pantograph. The effect of steady arm damping on the current collection quality of double pantographs-catenary is investigated through 11 numerical examples with the damping from 0 to 250 Ns/m. In the simulation, the double pantographs-catenary system used in Beijing-Tianjin High-speed line is adopted. The double pantographs interval is 200 m and the train speed is 350 km/h. The resulting contact force standard deviations $\sigma$ with different steady arm damping are presented in Tab. 8. When the steady arm damping is 50 Ns/m, the resultant $\sigma$ of both the trailing and leading pantographs are the lowest among all the cases. Therefore the slight steady arm damping has a positive effect on the current collection quality of the leading and trailing pantographs. However, when the steady arm damping is larger than 50 Ns/m, it behaves like a hard spot, and increase the $\sigma$ of the leading pantograph. Especially when the steady arm damping is larger than 200 Ns/m, it totally has a negative effect on the current collection quality of both the leading and trailing pantographs.

## VII.    CONCLUSION

This paper investigates the effective measures to improve the current collection quality of the double pantographs-catenary system. A double-pantographs-catenary model is established by FEM and its accuracy is verified by EN 50318 released in 2018. Based on the analysis of the contact wire uplift response with a single moving force, the deterioration mechanism of the current collection quality of the trailing pantograph is revealed. The results indicate that the bad interval coincidently appears at the velocity peak of the contact wire uplift, whereas, the good interval appears at the valley value of the contact wire uplift velocity. Addressing the shortcomings of the previous studies, the formula for the optimal double-pantographs interval is proposed, which can be used to determine the good and bad intervals for the double pantographs. In the proposed formula, the train speed, the length of passing stage $L_c$ and the frequency of the post-passage stage $f_c$ are the key parameters. Through a number of simulations with different types of double pantographs-catenary systems, the validation of the proposed formula is verified. Apart from the measures to optimise the pantographs interval, the effect of the steady arm damping on the double pantographs-catenary interaction performance is investigated. The results show that the slight steady arm damping has a positive effect on the performance of the double pantographs-catenary interaction.

## REFERENCES

[1]    Z. Liu, Y. Song, Y. Han, H. Wang, J. Zhang, and Z. Han, "Advances of research on high-speed railway catenary," *J. Mod. Transp.*, vol. 26, no. 1, pp. 1–23, 2018.

[2]    S. Bruni, G. Bucca, M. Carnevale, A. Collina, and A. Facchinetti, "Pantograph–catenary interaction: recent achievements and future research challenges," *Int. J. Rail Transp.*, vol. 6, no. 2, pp. 57–82, 2018.

[3]    C. Mu, Z. Ni, C. Sun, and H. He, "Air-Breathing Hypersonic Vehicle Tracking Control Based on Adaptive Dynamic Programming," *IEEE Trans. Neural Networks Learn. Syst.*, vol. 28, no. 3, pp. 584–598, 2017.

[4]    C. Mu, C. Sun, and W. Xu, "Fast sliding mode control on air-breathing hypersonic vehicles with transient response analysis," *Proc. Inst. Mech. Eng. Part I J. Syst. Control Eng.*, vol. 230, no. 1, pp. 23–34, Jan. 2016.

[5]    S. Bruni *et al.*, "The results of the pantograph-catenary interaction benchmark," *Veh. Syst. Dyn.*, vol. 53, no. 3, pp. 412–435, 2015.

[6]    Y. Song, Z. Liu, H. Wang, X. Lu, and J. Zhang, "Nonlinear modelling of high-speed catenary based on analytical expressions of cable and truss elements," *Veh. Syst. Dyn.*, vol. 53, no. 10, pp. 1455–1479, 2015.

[7]    J. Pombo and J. Ambrósio, "Influence of pantograph suspension characteristics on the contact quality with the catenary for high speed trains," *Comput. Struct.*, vol. 110–111, pp. 32–42, 2012.

[8]    P. Nåvik, A. Rønnquist, and S. Stichel, "Variation in predicting pantograph–catenary interaction contact forces, numerical simulations and field measurements," *Veh. Syst. Dyn.*, vol. 55, no. 9, pp. 1265–1282, 2017.

[9]    Y. Song, Z. Liu, Z. Xu, and J. Zhang, "Developed moving mesh method for high-speed railway pantograph-catenary interaction based on nonlinear finite element procedure," *Int. J. Rail Transp.*, vol. 7, no. 3, pp. 173–190, 2019.

[10]    J. R. Jimenez-Octavio, A. Carnicero, C. Sanchez-Rebollo, and M. Such, "A moving mesh method to deal with cable structures subjected to moving loads and its application to the catenary-pantograph dynamic interaction," *J. Sound Vib.*, vol. 349, pp. 216–229, 2015.

[11]    S. Gregori, M. Tur, A. Pedrosa, J. E. Tarancón, and F. J.

Fuenmayor, "A modal coordinate catenary model for the real-time simulation of the pantograph-catenary dynamic interaction," *Finite Elem. Anal. Des.*, vol. 162, no. January, pp. 1–12, 2019.

[12] Y. Lei, W. Xu, C. Mu, Z. Zhao, H. Li, and Z. Li, "New Hybrid Damping Strategy for Grid-Connected Photovoltaic Inverter with LCL Filter," *IEEE Trans. Appl. Supercond.*, vol. 24, no. 5, pp. 1–8, 2014.

[13] P. Nåvik, A. Rønnquist, and S. Stichel, "Identification of system damping in railway catenary wire systems from full-scale measurements," *Eng. Struct.*, vol. 113, pp. 71–78, 2016.

[14] D. Zou, W. H. Zhang, R. P. Li, N. Zhou, and G. M. Mei, "Determining damping characteristics of railway-overhead-wire system for finite-element analysis," *Veh. Syst. Dyn.*, vol. 54, no. 7, pp. 902–917, 2016.

[15] Y. Song, Z. Liu, F. Duan, X. Lu, and H. Wang, "Study on Wind-Induced Vibration Behavior of Railway Catenary in Spatial Stochastic Wind Field Based on Nonlinear Finite Element Procedure," *J. Vib. Acoust.*, vol. 140, no. 1, p. 11010, 2017.

[16] Y. Song, Z. Liu, H. Wang, X. Lu, and J. Zhang, "Nonlinear analysis of wind-induced vibration of high-speed railway catenary and its influence on pantograph–catenary interaction," *Veh. Syst. Dyn.*, vol. 54, no. 6, pp. 723–747, 2016.

[17] Y. Song, Z. Liu, H. Wang, J. Zhang, X. Lu, and F. Duan, "Analysis of the galloping behaviour of an electrified railway overhead contact line using the non-linear finite element method," *Proc. Inst. Mech. Eng. Part F J. Rail Rapid Transit*, vol. 232, no. 10, pp. 2339–2352, 2018.

[18] Z. Wang, Y. Song, Z. Yin, R. Wang, and W. Zhang, "Random response analysis of axle-box bearing of a high-speed train excited by crosswinds and track irregularities," *IEEE Trans. Veh. Technol.*, vol. 68, no. 11, pp. 1–1, 2019.

[19] S. Chen and F. Sha, "Three types of electromagnetic noise between pantograph and catenary," *Proc. - 2009 3rd IEEE Int. Symp. Microwave, Antenna, Propag. EMC Technol. Wirel. Commun. MAPE 2009*, no. 2008, pp. 40–43, 2009.

[20] Z. Xu, G. Gao, Z. Yang, W. Wei, and G. Wu, "An Online Monitoring Device for Pantograph Catenary Arc Temperature Detect Based on Atomic Emission Spectroscopy," *ICHVE 2018 - 2018 IEEE Int. Conf. High Volt. Eng. Appl.*, pp. 1–4, 2019.

[21] Y. Song, Z. Liu, F. Duan, Z. Xu, and X. Lu, "Wave propagation analysis in high-speed railway catenary system subjected to a moving pantograph," *Appl. Math. Model.*, vol. 59, pp. 20–38, Jul. 2018.

[22] E. Karakose, M. T. Gencoglu, M. Karakose, I. Aydin, and E. Akin, "A new experimental approach using image processing-based tracking for an efficient fault diagnosis in pantograph-catenary systems," *IEEE Trans. Ind. Informatics*, vol. 13, no. 2, pp. 635–643, 2017.

[23] H. Wang, Z. Liu, A. Nunez, and R. Dollevoet, "Entropy-Based Local Irregularity Detection for High-Speed Railway Catenaries With Frequent Inspections," *IEEE Trans. Instrum. Meas.*, vol. 68, no. 10, pp. 3536–3547, 2018.

[24] X. Lu, Z. Liu, Y. Song, H. Wang, J. Zhang, and Y. Wang, "Estimator-based multiobjective robust control strategy for an active pantograph in high-speed railways," *Proc. Inst. Mech. Eng. Part F J. Rail Rapid Transit*, vol. 232, no. 4, pp. 1064–1077, Apr. 2018.

[25] Y. Song, H. Ouyang, Z. Liu, G. Mei, H. Wang, and X. Lu, "Active control of contact force for high-speed railway pantograph-catenary based on multi-body pantograph model," *Mech. Mach. Theory*, vol. 115, pp. 35–59, 2017.

[26] Y. Song, Z. Liu, H. Ouyang, H. Wang, and X. Lu, "Sliding Mode Control with PD Sliding Surface for High-Speed Railway Pantograph-Catenary Contact Force under Strong Stochastic Wind Field," *Shock Vib.*, vol. 2017, 2017.

[27] G. Bucca *et al.*, "Adoption of different pantographs preloads to improve multiple collection and speed up existing lines," *Veh. Syst. Dyn.*, vol. 50, no. SUPPL. 1, pp. 403–418, 2012.

[28] J. Ambrósio, J. Pombo, M. Pereira, P. Antunes, and A. Mósca, "A computational procedure for the dynamic analysis of the catenary-pantograph interaction in high-speed train," *J. Theor. Appl. Mech.*, vol. 50, no. 3, pp. 681–699, 2012.

[29] W. Zhang, N. Zhou, R. Li, G. Mei, and D. Song, "Pantograph and catenary system with double pantographs for high-speed trains at 350 km/h or higher," *J. Mod. Transp.*, vol. 19, no. 1, pp. 7–11, 2011.

[30] Z. Liu, P. A. Jönsson, S. Stichel, and A. Rønnquist, "On the implementation of an auxiliary pantograph for speed increase on existing lines," *Veh. Syst. Dyn.*, vol. 54, no. 8, pp. 1077–1097, 2016.

[31] *European Committee for Electrotechnical Standardization EN50318. Railway applications - Current collection systems - Validation of simulation of the dynamic interaction between pantograph and overhead contact line.* 2018.

[32] I. M. Smith, D. V. Griffiths, and L. Margetts, *Programming the Finite Element Method.* Wiley, 2013.

[33] *European Committee for Electrotechnical Standardization EN50367-2012 Railway applications. Current collection systems.Technical criteria for the interaction between pantograph and overhead line (to achieve free access).* 2012.

**Zhao Xu** (S'19) received the B.S degree in Engineering mechanics from Southwest Jiaotong University, Sichuan, China, in 2016, where he is currently pursuing the Ph.D. degree with the school of Electrical Engineering, Southwest Jiaotong University. His research interests include finite element modeling, structural dynamics, and their applications in the design and maintenance of railway pantograph-catenary system.

**Yang Song** (S'16–M'19) received the Ph.D. degree in electrical engineering from Southwest Jiaotong University, Sichuan, China, in 2018. He worked as a Research Fellow with the Institute of Railway Research, School of Computing and Engineering, University of Huddersfield, UK from 10/2018 to 09/2019. He is currently a Postdoctoral Fellow at Department of Structural Engineering, Norwegian University of Technology, Norway. His research interests involve the assessment of railway pantograph-catenary interaction, the wind-induced vibration of long-span structures of railway transportation, and the coupling dynamics in railway engineering.

**Zhigang Liu** (M'06–SM'16) received his Ph.D. degree in Power System and its Automation from Southwest Jiaotong University of China in 2003. He is currently a full Professor of School of Electrical Engineering, Southwest Jiaotong University. His research interests are the electrical relationship of EMUs and traction, detection and assessment of pantograph-catenary in high-speed railway.

Dr. Liu was elected as a Fellow of The Institution of Engineering and Technology (IET) in 2017. He received the IEEE TIM's Outstanding Associate Editors for 2019 and the Outstanding Reviewer of the IEEE Transactions on Instrumentation and Measurement for 2018. He is an Associate Editor of IEEE Transactions on Neural Networks and Learning Systems, IEEE Transactions on Vehicular Technology, IEEE Transactions on Instrumentation and Measurement and IEEE Access.